materials

MDPI

Article

Effect of $LaCoO_3$ Synthesized via Solid-State Method on the Hydrogen Storage Properties of MgH_2

Noratiqah Sazelee [1], Muhamad Faiz Md Din [2], Mohammad Ismail [1,*], Sami-Ullah Rather [3], Hisham S. Bamufleh [3], Hesham Alhumade [3], Aqeel Ahmad Taimoor [3] and Usman Saeed [3]

1 Energy Storage Research Group, Faculty of Ocean Engineering Technology and Informatics, University Malaysia Terengganu, Kuala Terengganu 21030, Malaysia; atiqahsazelee19@gmail.com
2 Department of Electrical and Electronic Engineering, Faculty of Engineering, National Defence University of Malaysia, Kem Sungai Besi, Kuala Lumpur 57000, Malaysia; faizmd@upnm.edu.my
3 Department of Chemical and Materials Engineering, King Abdulaziz University, P.O. Box 80204, Jeddah 21589, Saudi Arabia; rathersami@kau.edu.sa (S.-U.R.); hbamufleh@kau.edu.sa (H.S.B.); halhumade@kau.edu.sa (H.A.); ataimoor@kau.edu.sa (A.A.T.); umsaeed@kau.edu.sa (U.S.)
* Correspondence: mohammadismail@umt.edu.my; Tel.: +60-96-683-487

Abstract: One of the ideal energy carriers for the future is hydrogen. It has a high energy density and is a source of clean energy. A crucial step in the development of the hydrogen economy is the safety and affordable storage of a large amount of hydrogen. Thus, owing to its large storage capacity, good reversibility, and low cost, Magnesium hydride (MgH_2) was taken into consideration. Unfortunately, MgH_2 has a high desorption temperature and slow ab/desorption kinetics. Using the ball milling technique, adding cobalt lanthanum oxide ($LaCoO_3$) to MgH_2 improves its hydrogen storage performance. The results show that adding 10 wt.% $LaCoO_3$ relatively lowers the starting hydrogen release, compared with pure MgH_2 and milled MgH_2. On the other hand, faster ab/desorption after the introduction of 10 wt.% $LaCoO_3$ could be observed when compared with milled MgH_2 under the same circumstances. Besides this, the apparent activation energy for MgH_2–10 wt.% $LaCoO_3$ was greatly reduced when compared with that of milled MgH_2. From the X-ray diffraction analysis, it could be shown that in-situ forms of MgO, CoO, and La_2O_3, produced from the reactions between MgH_2 and $LaCoO_3$, play a vital role in enhancing the properties of hydrogen storage of MgH_2.

Keywords: cobalt lanthanum oxide; magnesium hydride; metal oxide; solid-state hydrogen storage

Citation: Sazelee, N.; Md Din, M.F.; Ismail, M.; Rather, S.-U.; Bamufleh, H.S.; Alhumade, H.; Taimoor, A.A.; Saeed, U. Effect of $LaCoO_3$ Synthesized via Solid-State Method on the Hydrogen Storage Properties of MgH_2. *Materials* **2023**, *16*, 2449. https://doi.org/10.3390/ma16062449

Academic Editors: Alessandro Dell'Era, Erwin Ciro Zuleta and Haralampos N. Miras

Received: 8 February 2023
Revised: 8 March 2023
Accepted: 14 March 2023
Published: 19 March 2023

1. Introduction

Hydrogen is increasingly seen as an energy carrier owing to its non-toxicity, abundant resources, positive environmental impact, and high energy density [1–3]. Nowadays, searching for effective hydrogen storage technologies is commonly recognized as one of the major difficulties faced by the hydrogen economy [4,5]. Solid-state hydrogen storage materials have drawn a significant amount of interest because of their safety consideration, cheapness, and high gravimetric capacity [6]. Over the past decade, MgH_2 gained research interest due to its outstanding reversibility, low cost, non-toxicity, an abundance of resources, and high gravimetric hydrogen capacity (7.60 wt.%) [7–9]. Fortunately, practical applications of MgH_2 are severely restricted by the slow reaction kinetics and high dissociation temperature [10–12]. Recently, significant improvements have been made by producing nanocrystalline MgH_2 powders by the addition of metal oxide additives such as Nb_2O_5 [13], TiO_2 [14], $CoTiO_3$ [15], $CoMoO_4$ [16], and $MnMoO_4$ [17], through ball milling method to enhance hydrogen storage performance of MgH_2. Rare earth metals are considered as one of the most intriguing additives/catalysts used in solid-state materials. For example, Ismail [18] found that after the addition of 10 wt.% $LaCl_3$ into MgH_2, hydrogen started to be released at 300 °C, 50 °C lower than with milled MgH_2. It is revealed that the formation of $MgCl_2$ and Mg–La alloy during the heating process of the composites

gives a vital role in enhancing the performance of hydrogen storage of MgH_2. In our previous study [19], adding 10 wt.% $LaFeO_3$ to MgH_2 positively affected the hydrogen sorption properties of MgH_2. Compared with pure MgH_2, the introduction of 10 wt.% of $LaFeO_3$ reduced the desorption temperature by 120 °C. Further studies have exposed that ab/desorption kinetics of MgH_2 were improved by the formation of Fe, MgO, and La_2O_3 phases during the heating process. For instance, Soni et al. [20] introduced LaF_3 into MgH_2 and proved that the samples started to release hydrogen at 320 °C, 40 °C lower than with milled MgH_2. In addition, milled MgH_2 absorbed only 2.00 wt.% hydrogen in 2.5 min, while MgH_2 + LaF_3 could absorb 4.90 wt.% of H_2 under the same circumstances. Wu et al. [21] reported that adding $LaNiO_3$ significantly enhanced the desorption and absorption kinetics of MgH_2. Further investigation revealed that in situ formations of Mg_2NiH_4 and LaH_3 have a synergistic effect that can serve as a "hydrogen pump", hence enhancing the sorption kinetics of MgH_2. The research led by Zhang and co-workers [22] discovered that after introducing $LaNi_{4.5}Mn_{0.5}$ to MgH_2, excellent catalytic activity was observed. Interestingly, at 300 °C, the composites could desorb 6.60 wt.% of H_2 in less than 360 s.

Besides this, according to Juahir et al. [23], doping MgH_2 with Co_2NiO lowered the starting hydrogen release and enhanced the ab/desorption kinetics of MgH_2. According to their research, the formation of $Co_{1.29}Ni_{1.71}O_4$ and Mg–Co alloy served as a real catalyst in enhancing the hydrogen sorption properties of MgH_2. In comparison to other ferrites ($ZnFe_2O_4$, $CoFe_2O_4$, $MnFe_2O_4$, and $Mn_{0.5}Zn_{0.5}O_4$), Zhang et al. [24] came to the finding that $CoFe_2O_4$ had the best catalytic performance in enhancing the hydrogen storage performance of MgH_2. Furthermore, Cabo et al. [25] discovered that the addition of Co_3O_4 and $NiCo_2O_4$ additives decreased the starting desorption temperature of MgH_2. In particular, Mandzhukova et al. [26] analyzed the effect of $NiCo_2O_4$ on the kinetic performance of the Mg/MgH_2 system, and revealed that the kinetic properties of Mg were drastically enhanced. Liu et al. [27] used a reduction reaction method to synthesize Co@CNT and found that the doped samples began to release hydrogen at 324 °C, which was lower than that of the bulk samples (420 °C). Further research indicated that the energy barrier for hydrogen dissociation can be substantially reduced by Co and Co(II).

Motivated by previous research, two promising materials (La and Co) clearly demonstrate that $LaCoO_3$ improves hydrogen ab/desorption kinetics and lowers the MgH_2 desorption temperature. In this paper, different amounts of $LaCoO_3$ were milled together to make MgH_2–x wt.% $LaCoO_3$ (where x is 5, 10, 15, and 20) composites. $LaCoO_3$ was used as an additive to see how this material affected the hydrogen sorption properties of MgH_2. To date, this is the first research into the hydrogen storage performance of $MgH_2/LaCoO_3$ composites for solid-state materials.

2. Materials and Methods

The $LaCoO_3$ material was synthesized by using citric acid (≥98% pure; Sigma Aldrich, St. Louis, MO, USA), lanthanum oxide (≥99.9% pure; Aldrich Chemical Compound, Milwaukee, WI, USA), and pure cobalt oxide (99.99% pure; Sigma Aldrich, St. Louis, MO, USA) as starting materials with 0.121 g, 0.081 g, and 0.040 g respectively. The powders were mixed and thoroughly ground in an agate mortar. The solid mixture was then placed into crucibles made of alumina and calcined at 950 °C in a furnace for 5 h. In a planetary ball mill (NQM-0.4), using stainless steel vials and 4 balls at 400 rpm with a 40:1 ball-to-powder ratio, the various weight percentage (5, 10, 15, and 20) of $LaCoO_3$ were milled together with MgH_2 (≥95% pure; Sigma Aldrich, St. Louis, MO, USA). This milling approach was carried out for 1 h in different directions (milling = 15 min, rest = 2 min, mill again = 15 min). In an argon atmosphere, the MBRAUN UNIlab glove box was used for all the preparations (including weighing).

Sievert-type pressure composition temperature (Advanced Materials Corporation, Pittsburgh, PA, USA) was used to investigate the temperature-programmed-desorption (TPD) and hydrogen ab/desorption kinetics for all of the samples. Approximately,

400 mg of the samples were used in each test. All the samples were heated to 450 °C from ambient temperature for the TPD analyses at a rate of 5 °C/min. The absorption kinetics were carried out at 250 °C (33.0 atm), meanwhile, the desorption kinetics were evaluated at 300 °C (1.0 atm). To observe the hydrogen desorption behavior of MgH_2, differential scanning calorimetry (DSC) was performed on a Mettler Toledo TGA/DSC 1. The samples were heated from 30 to 500 °C at rates of 15, 20, 25, and 30 °C/min under constant argon flow (50 mL). An alumina crucible in a glove box was filled with about 3–5 mg, and to prevent oxidation, the samples were then placed in a sealed glass bottle. To scrutinize the phase structure of the samples, X-ray diffraction (XRD) spectra were recorded in the range of 20°–80° using Cu-Kα radiation to analyze the phase structure of each sample. Scan speeds of 2.00°/min were used for θ–2θ scans. Prior to this, a small portion of the samples was evenly distributed on a sample holder and sealed with scotch tape to prevent oxidation.

The morphology of the samples was examined using scanning electron microscopy (SEM; JEOL, Akishima, Tokyo, Japan) (JSM-6360LA). In a vacuum state, the gold spray was applied to the samples after being prepared on carbon tape. Moreover, to further examine the sample's chemical bond, a Shimadzu IRTracer-100, Kyoto, Japan Fourier Transform Infrared spectroscopy was used. Attenuated total reflectance (ATR) was used to measure the spectra at room temperature for 40 scans, between 2000 and 400 cm^{-1}, with a resolution of 4 cm^{-1}. At room temperature, Raman spectroscopy was performed using Renishaw Raman spectroscopy (532 nm radiation) extended with 0.1% power laser measurement.

3. Results and Discussion

Calcining the samples at 950 °C for 5 h yielded well-crystallized pure $LaCoO_3$ (JCPDF: 25-1060), in the rhombohedral structure as shown in Figure 1a. All diffraction lines corresponding to (012), (110), (202), (006), (024), (122), (116), (214), (018), (220), (208), (306), and (134) planes were closely matched to 23.25°, 32.89°, 40.64°, 41.32°, 47.49°, 53.24°, 53.78°, 58.79°, 59.73°, 68.93°, 69.90°, 74.32°, and 78.74°, respectively, and were all closely matched to the previously reported data [28,29]. The crystallite sizes (L) were estimated at 20.85 nm, through the Scherrer formula as shown in Equation (1) below:

$$L = K\lambda/\beta \cos \theta \quad (1)$$

where shape factor K = 0.94 constant, λ = X-ray used (0.154 nm), β (physical broadening) = full width at half the maximum, and θ = angle of Bragg's diffraction. The FTIR transmission of $LaCoO_3$ is indicated in Figure 1b. A peak at 508 cm^{-1} is ascribed to the Co–O bond as reported by Sarker and Razzaque [28], and Worayingyong et al. [30]. The La–O bond as confirmed by Radev et al. [31], corresponds to the peak at 410 cm^{-1}. The Raman spectra shown in Figure 1c illustrates typical characteristics of $LaCoO_3$ at 478 cm^{-1}, confirming the formation of La–O [32]. It can be evidenced that the pure $LaCoO_3$ was successfully synthesized by using the solid-state method based on the results of XRD, FTIR, and Raman spectroscopy. Meanwhile, Figure 1d shows the morphology of $LaCoO_3$, where the agglomeration of particles of different sizes can be seen as indicated in a previous study [33]. Besides this, the particle sizes distribution (PSD) of the $LaCoO_3$ particle was calculated by using ImageJ (version 2022). Based on Figure 1e below, the PSD of $LaCoO_3$ was 82.71 μm.

The impact of $LaCoO_3$ on the desorption temperature of MgH_2 was measured using the TPD profile of gas desorption from the samples, as displayed in Figure 2a. Pure MgH_2 and milled MgH_2 both had onset desorption temperatures of 420 °C and 350 °C, respectively. It was discovered that the milling process had an impact on the decomposition of MgH_2. According to Sokano et al. [34], milled MgH_2 has a lower onset desorption temperature, which is 328 °C, compared with that of pure MgH_2 (418 °C). However, the onset desorption temperature was shifted from 350 °C to a starting temperature below 325 °C when different weight percent of $LaCoO_3$ were added to MgH_2. The onset desorption temperature of 5, 10, 15, and 20 wt.% of $LaCoO_3$ with MgH_2 was 316, 322, 310, and 323 °C, respectively. Meanwhile, the desorption capacity of 5, 10, 15, and 20 wt.%

of $LaCoO_3$ with MgH_2 was 6.57, 6.06, 6.03, and 5.30 wt.%, respectively. A study led by Pandey et al. [35] proved that adding TiO_2 to MgH_2 lowered the onset desorption temperature to 335 °C, 55 °C lower than that of pure MgH_2. Despite the fact that adding $LaCoO_3$ lowered the desorption temperature of MgH_2, the hydrogen desorption capacity of xwt.% of $LaCoO_3$ (where x is 5, 10, 15, and 20 wt.%) with MgH_2 decreased due to the dead weight of $LaCoO_3$.

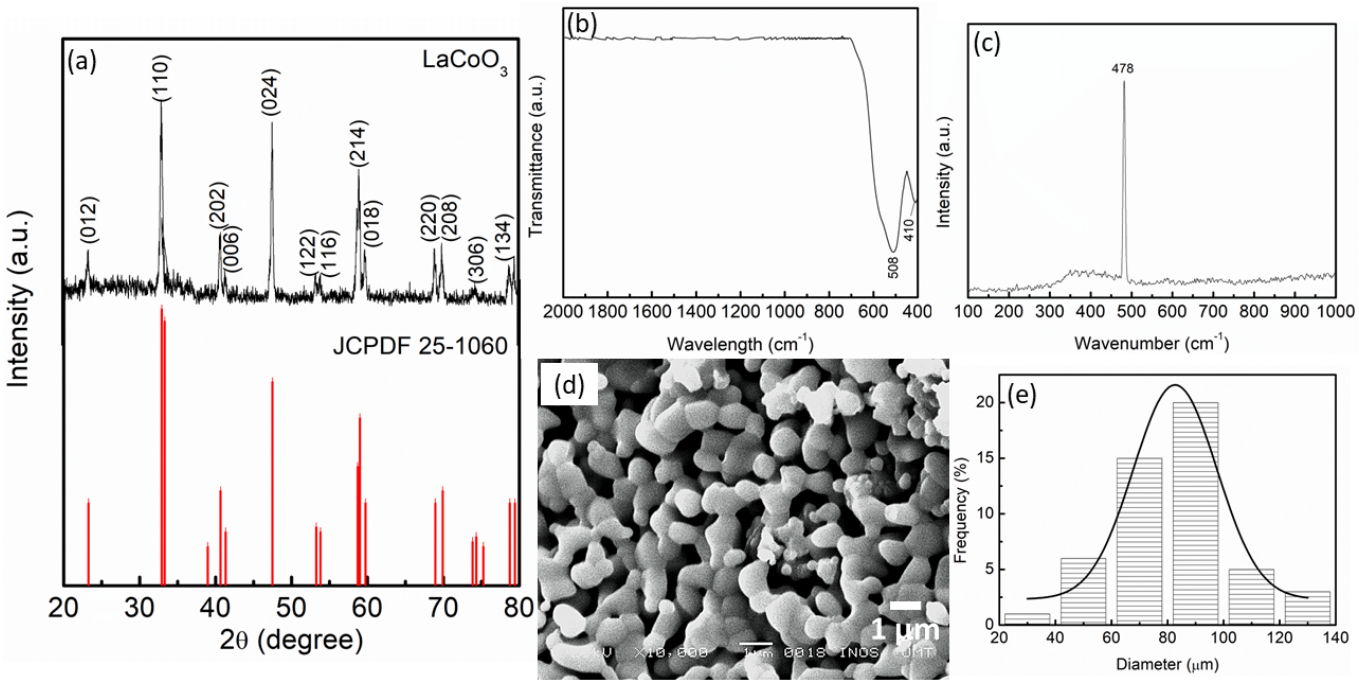

Figure 1. (**a**) XRD pattern, (**b**) FTIR spectra, (**c**) Raman spectra, (**d**) SEM images, and (**e**) PSD of $LaCoO_3$.

The isothermal absorption measurement of the milled MgH_2 and xwt.% of $LaCoO_3$ (where x is 5, 10, 15, and 20 wt.%) with MgH_2 was further conducted under 33.0 atm at 250 °C, as depicted in Figure 2b. The result proved that adding 5, 10, 15, and 20 wt.% of $LaCoO_3$ with MgH_2 could absorb 7.30, 7.30, 6.99, and 5.49 wt.%, respectively, within 20 min. Meanwhile, milled MgH_2 could only absorb 6.68 wt.% under the same circumstances. The amount of hydrogen absorption for 20 wt.% of $LaCoO_3$ with MgH_2 was lower by 1.19 wt.%, compared with that of milled MgH_2. This was due to the possibility that too much additive in the composite may block the diffusion path of hydrogen [36]. A previous study reported by Sulaiman et al. [37] indicated that the amount of Na_3FeF_6 affects the hydrogen absorption behavior of MgH_2. The addition of excess Na_3FeF_6 catalyst into MgH_2 obstructs the hydrogen diffusion by blocking the diffusion path, which limits the Mg-H reaction. However, faster absorption kinetics of MgH_2 could be seen within 4 min after the addition of 20 wt.% $LaCoO_3$. As evidenced by the above experimental results, the hydrogen absorption kinetics of MgH_2 can be improved by the presence of $LaCoO_3$.

To compare hydrogen desorption properties of different weight percentages of $LaCoO_3$ with MgH_2 and milled MgH_2, an isothermal desorption test was conducted at 300 °C for 1 h, as presented in Figure 2c. It is clear that MgH_2–$LaCoO_3$ composites demonstrated faster desorption kinetics than milled MgH_2. An amount of 5 wt.% of $LaCoO_3$ with MgH_2, and 10 wt.% of $LaCoO_3$ with MgH_2 released H_2 at approximately 2.46 and 3.24 wt.%, respectively. In addition, 15 wt.% of $LaCoO_3$ with MgH_2, and 20 wt.% of $LaCoO_3$ with MgH_2 desorbed 2.01 wt.% and 4.53 wt.% of H_2, respectively. However, milled MgH_2 only released 0.34 wt.% of H_2 under the same circumstances. Table 1 summarizes the onset desorption temperature, the capacity of absorption kinetics at 250 °C, and desorption kinetics at 300 °C for pure MgH_2, milled MgH_2, and composites of different $LaCoO_3$ weight percent-

ages with MgH_2. Considering the onset desorption temperature, absorption and desorption kinetics of each sample, 10 wt.% of $LaCoO_3$ with MgH_2 composites were chosen for further investigation.

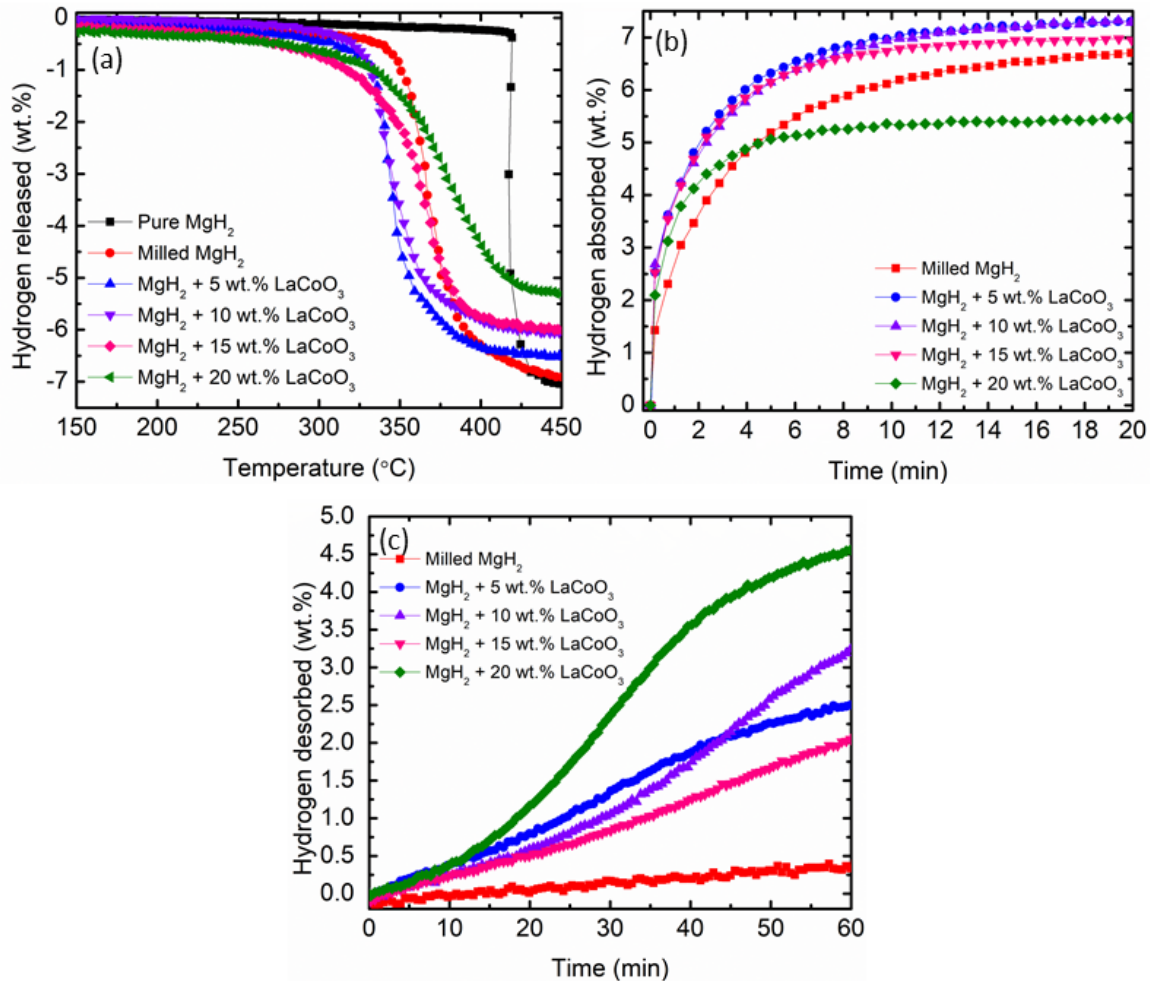

Figure 2. (**a**) Temperature-programmed desorption, (**b**) Isothermal absorption kinetics at 250 °C, and (**c**) Isothermal desorption kinetics at 300 °C.

Table 1. Temperature-programmed desorption, absorption and desorption capacity of each sample.

Samples	Onset Desorption Temperature (°C)	Absorption Capacity (wt.%)	Desorption Capacity (wt.%)
Pure MgH_2	420	-	-
Milled MgH_2	350	6.68	0.34
5 wt.% $LaCoO_3$ with MgH_2	316	7.30	2.46
10 wt.% $LaCoO_3$ with MgH_2	322	7.30	3.24
15 wt.% $LaCoO_3$ with MgH_2	310	6.99	2.04
20 wt.% $LaCoO_3$ with MgH_2	323	5.49	4.53

To obtain a greater understanding of the kinetic mechanism in hydrogen storage materials, kinetic models were used to describe absorption and desorption behaviors. In this study, the kinetic mechanism was investigated by using the Johnson-Mehl-Avrami (JMA) and Contracting Volume (CV) equations as can be seen in Table 2 [38].

Table 2. The equations for kinetic models used for absorption and desorption kinetics of this study.

Integrated Equation	Model
$\alpha = kt$	Surface-controlled (chemisorption)
$[-\ln(1-\alpha)]^{1/2} = kt$	JMA, n = 2 (e.g., two-dimensional growth of existing nuclei with constant interface velocity)
$[-\ln(1-\alpha)]^{1/3} = kt$	JMA, n = 3 (e.g., two-dimensional growth of existing nuclei with constant interface velocity)
$1-(1-\alpha)^{1/3} = kt$	CV 2D: contracting volume, three-dimensional growth with constant interface velocity
$1-(2\alpha/3)-(1-\alpha)^{2/3} = kt$	CV 3D: contracting volume, three-dimensional growth diffusion controlled with decreasing interface velocity

Where k = reaction rate constant, t = time, and α = reacted fraction.

The absorption and desorption kinetic curves for 10 wt.% $LaCoO_3$ with MgH_2 composites are illustrated in Figure 3a,b below. The kinetic curves for the composites were calculated for the reacted fraction in the range from 0 to 80%. Based on the figure below, the absorption process at 250 °C can be best described by the CV 3D decrease surface while the desorption process at 300 °C can be best described by the JMA 2D.

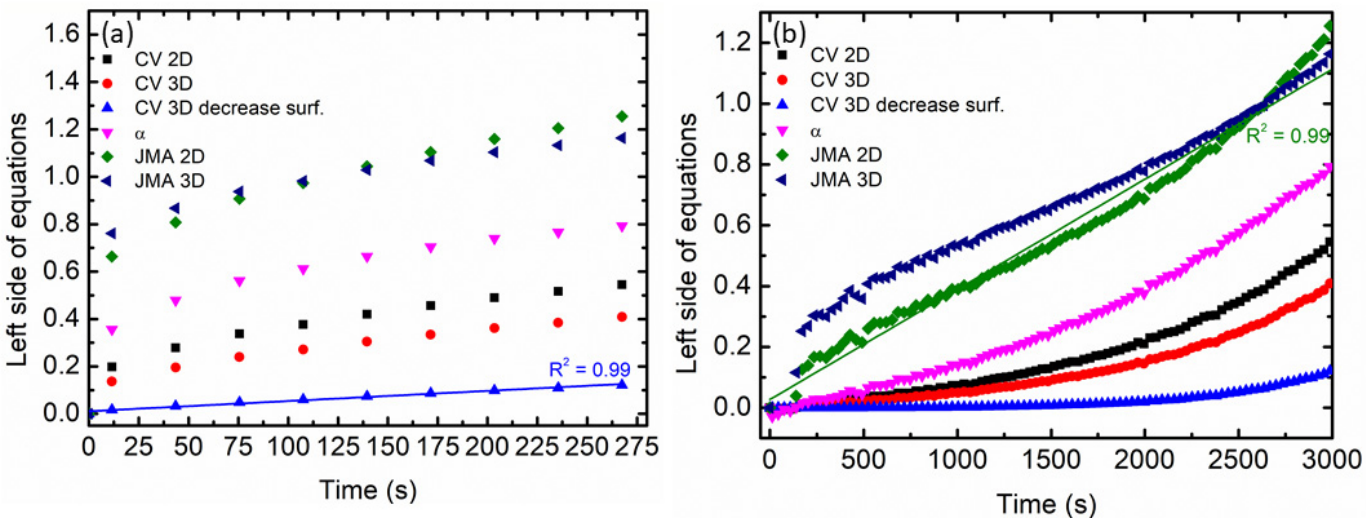

Figure 3. The resulting calculation of different kinetic equations is described in Table 2 for (**a**) absorption kinetics at 250 °C and (**b**) desorption kinetics at 300 °C of 10 wt.% of $LaCoO_3$ doped MgH_2.

DSC analyses were used to look into the effect of $LaCoO_3$ on the desorption kinetics of MgH_2. Figure 4a exhibits the DSC curves of milled MgH_2, while Figure 4b indicates the 10 wt.% of $LaCoO_3$ with MgH_2 composites heated at various heating rates. As the heating rises, the hydrogen desorption peaks move to a higher temperature. An endothermic peak for both samples was detected in Figure 4c for a heating rate of 25 °C/min, revealing that the decomposition from MgH_2 to Mg had occurred. As indicated in Figure 4c, the endothermic peak for milled MgH_2 was 433 °C, while the temperature was shifted to a lower temperature after 10 wt.% of $LaCoO_3$ was added (415 °C). From the results obtained for 10 wt.% of $LaCoO_3$ with MgH_2, the desorption peak temperature by DSC and TPD were 415 °C and 322 °C, respectively. This was due to the different atmospheres and heating rates as explained in our previous research [39,40]. A similar outcome had been observed by Verma et al. [41], which revealed that different desorption temperatures for DSC and TPD could be detected when the experiment was conducted under different circumstances.

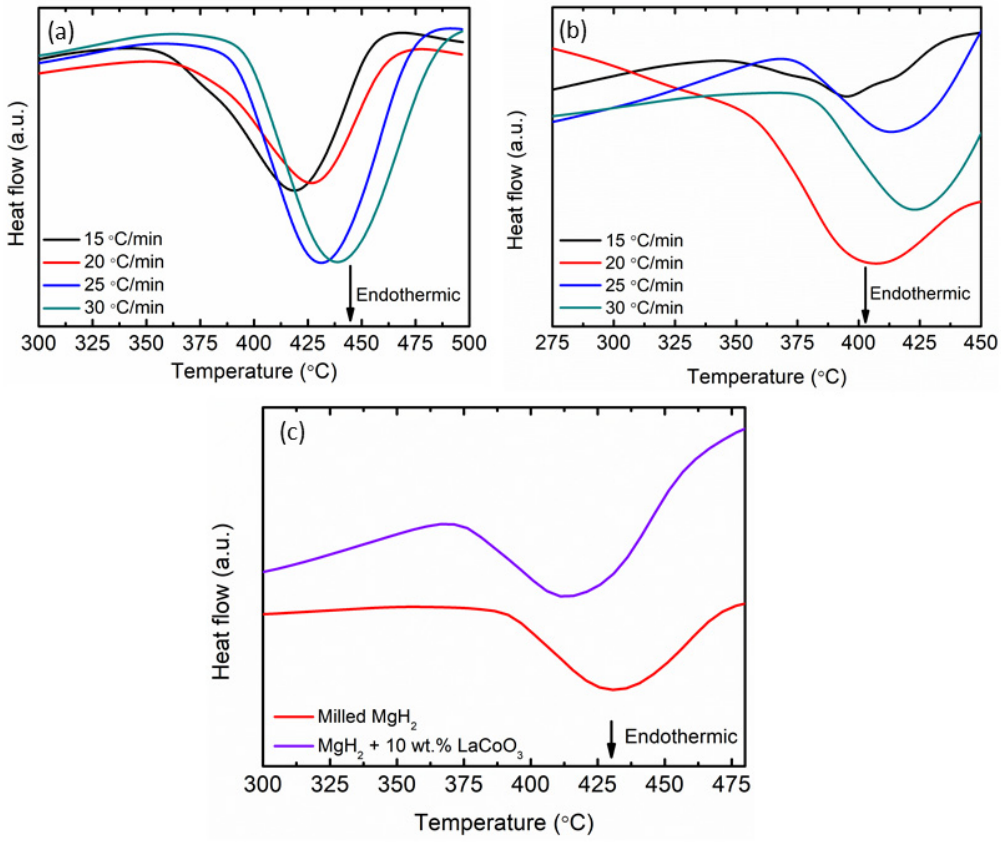

Figure 4. DSC curves of (**a**) milled MgH_2 at 15, 20, 25, and 30 °C/min, (**b**) 10 wt.% of $LaCoO_3$ with MgH_2 at 15, 20, 25, and 30 °C/min, and (**c**) milled MgH_2 and 10 wt.% of $LaCoO_3$ with MgH_2 at 25 °C/min.

The Kissinger method was used for both samples to evaluate the effect of $LaCoO_3$ additives on desorption apparent activation energy (E_A), as shown in Equation (2) below

$$\mathrm{In}\,[\beta/T_p{}^2] = -E_A/\mathrm{R}T_p + \mathrm{A} \quad (2)$$

where A = linear constant, T_p = peak temperature in the DSC curve, R = gas constant, and β = heating rate of the samples. Hence, the E_A of the thermal decomposition for 10 wt.% of $LaCoO_3$ with MgH_2 based on Equation (2) was approximately 90 kJ/mol, as demonstrated in Figure 5. Conversely, the E_A for milled MgH_2 was only 133 kJ/mol. The E_A of 10 wt.% of $LaCoO_3$ with MgH_2 was lower than those of the other additives from previous studies, such as MgH_2–$KNbO_3$ [42], MgH_2–Co@C [43], and MgH_2–$SrFe_{12}O_{19}$ [6]. According to the findings, overcoming the barrier for converting MgH_2 into Mg requires an E_A of 90 kJ/mol, in the presence of 10 wt.% $LaCoO_3$. It is also worth noting that $LaCoO_3$ additives lower the desorption peak temperature during the desorption processes of MgH_2.

The morphologies of pure MgH_2, milled MgH_2, and 10 wt.% of $LaCoO_3$ with MgH_2 were investigated by SEM as shown in Figure 6. The SEM of pure MgH_2 shown in Figure 6a revealed that the particles have a larger size and flakelike shapes, as reported by Czujko et al. [44]. Even though the samples were analyzed at different magnifications, as displayed in Figure 6b,d, both samples suggest that ball milling produces inhomogeneity, some agglomeration, and reduction in the MgH_2 samples caused by the ball collision. Smaller particle sizes for the milled MgH_2 suggests an enhancement in the desorption temperature of MgH_2. Besides, Shang and colleagues [45] indicated that the particle sizes in the submicron range can be achieved by milling Mg with or without the presence of additives. Compared with milled MgH_2 samples, it was obvious that particles the size of 10 wt.% of $LaCoO_3$ with MgH_2, as illustrated in Figure 6c,e, became smaller and less

agglomerated, which may accelerate the desorption and absorption kinetics of MgH_2 due to the increase of specific surface area, even when the samples were investigated at different magnifications. Chawla et al. [46] exposed that mechanical milling of Mg with $PdCl_2$ increases the surface area, resulting in a reduction in hydrogen atom diffusion length and an improvement in hydrogen ab/desorption kinetics. A similar outcome was also reported by Zinsou and co-workers [47] which also revealed that smaller particles are expected to release hydrogen at a lower temperature than samples that have larger particle sizes.

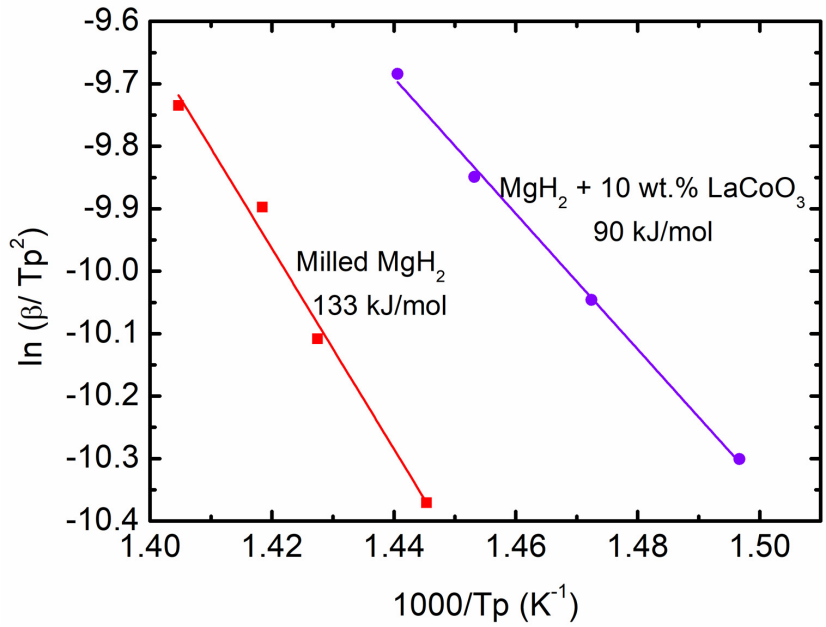

Figure 5. Activation energy of milled MgH_2 and 10 wt.% of $LaCoO_3$ with MgH_2.

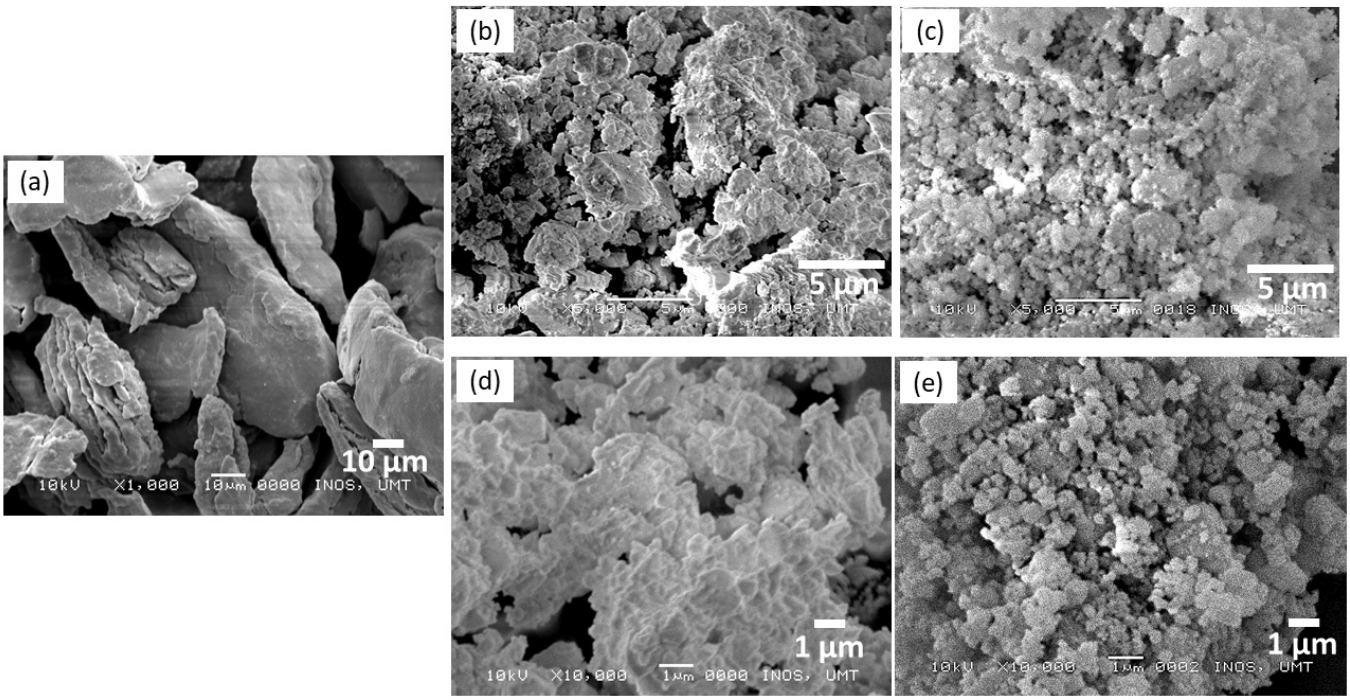

Figure 6. SEM images of (**a**) pure MgH_2, (**b**) milled MgH_2 at 5000× magnification, (**c**) 10 wt.% of $LaCoO_3$ with MgH_2 at 5000× magnification, (**d**) milled MgH_2 at 10,000× magnification, and (**e**) 10 wt.% of $LaCoO_3$ with MgH_2 at 10,000× magnification.

Particle size distribution was calculated by using Image J. The particle size distribution for pure MgH_2 is generally known to be 70 µm, as displayed in Figure 7a. Meanwhile, based on Figure 7b, the particle size distribution of MgH_2 started to decrease after MgH_2 was milled for 1 h (approximately 0.34 µm). Xiao and colleagues [48] have described that the particle size of commercial MgH_2 significantly reduced to ~300 nm after MgH_2 was milled. However, it is safer to assume that longer milling times would not result in a reduction in particle size as revealed by Rahmaninasab et al. [49]. Rahmaninasab et al. [49] also reported that the particle size of MgH_2 increased to 372 nm after the samples were milled for 40 h. Moreover, the particles of 10 wt.% of $LaCoO_3$ with MgH_2 were similar in size and less agglomerated, compared with those of milled MgH_2, and most of the particles were single particles with 0.13 µm for particles size distribution, as indicated in Figure 7c. The addition of additive and milling methods effectively alters the distribution of MgH_2. According to Si et al. [50], the increase in the small particles size was caused by the addition of Ni particles, which potentially improved the hydrogen storage performance of MgH_2. Therefore, adding 10 wt.% of $LaCoO_3$ reduces the particles size and shortens the diffusion length of MgH_2, and contributes in improving MgH_2 performance as observed.

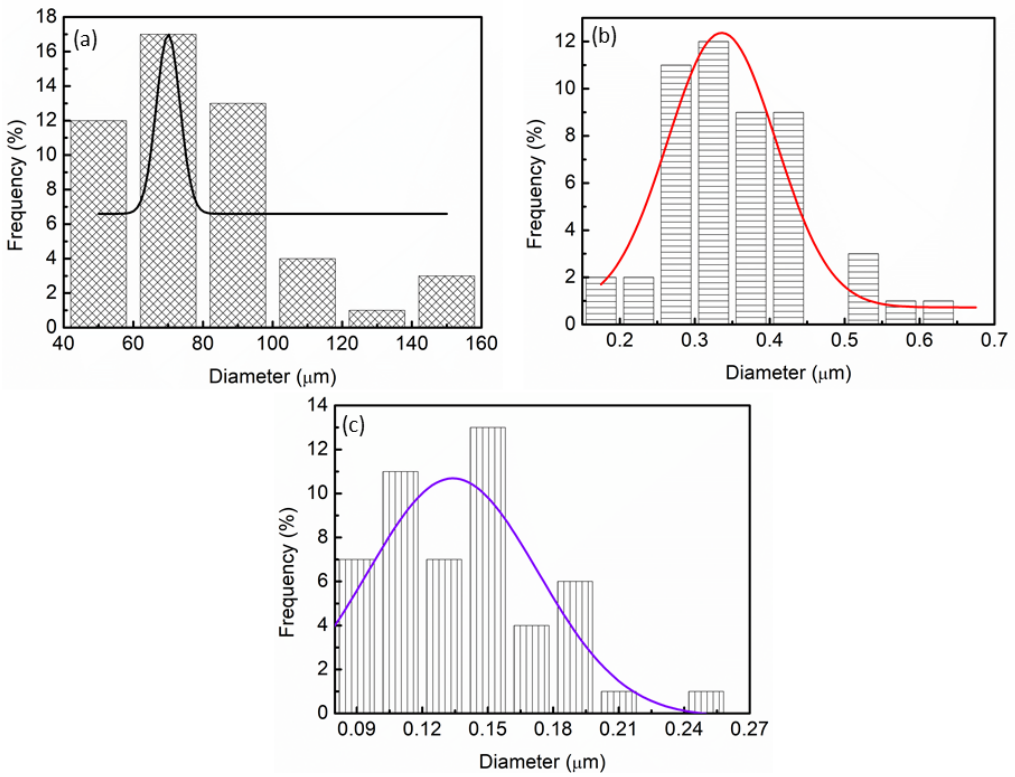

Figure 7. The PSD curves (**a**) pure MgH_2, (**b**) milled MgH_2, and (**c**) 10 wt.% of $LaCoO_3$ with MgH_2.

Figure 8 presents the FTIR spectra of the samples before and after being doped with 10 wt.% $LaCoO_3$. As seen from the figure below, the obvious signature bands for the Mg–H bending and Mg–H stretching are located between 400–800 cm^{-1} and 900–1200 cm^{-1}, respectively, for pure MgH_2, milled MgH_2, and 10 wt.% of $LaCoO_3$ with MgH_2. The results suggest that no obvious reactions occurred due to its relatively low content of $LaCoO_3$. Moreover, after adding 10 wt.% of $LaCoO_3$ to MgH_2, the bending bands of the samples tend to shift to lower wavenumbers, implying the weakness of the Mg–H bonds as proposed in a previous study [51].

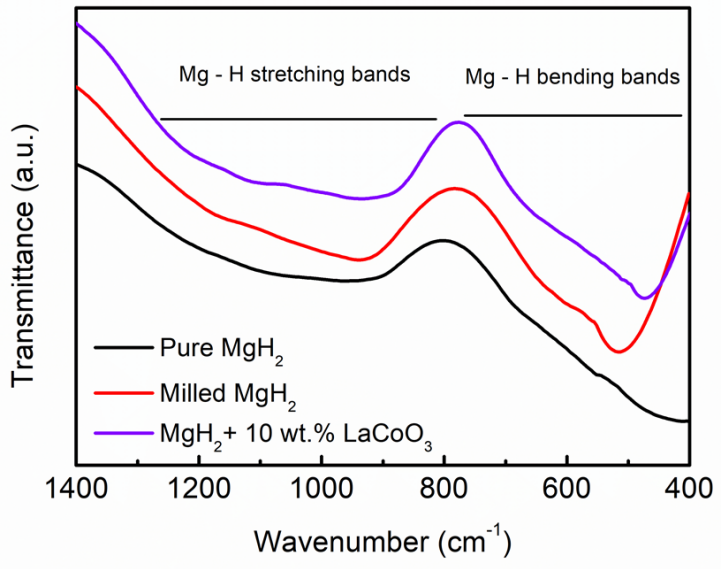

Figure 8. FTIR spectra of pure MgH_2, milled MgH_2, and 10 wt.% of $LaCoO_3$ with MgH_2.

The XRD pattern shown here in Figure 9 was used to clarify the mechanism of 10 wt.% of $LaCoO_3$ on MgH_2 hydrogen storage performance. After 10 wt.% of $LaCoO_3$ with MgH_2 was milled for 1 h, as shown in Figure 9a, the peaks of the composites mainly corresponded to parent materials which are MgH_2 and $LaCoO_3$, indicating that $LaCoO_3$ had not reacted with MgH_2 during the milling process. Based on Figure 9b, after the composites were heated up to 450 °C, MgH_2 peaks completely disappeared and transformed to Mg, implying that the decomposition process had occurred completely. A new peak of CoO, La_2O_3, and MgO was detected. The 10 wt.% of $LaCoO_3$ with MgH_2 during the absorption process at 250 °C had also been conducted, as shown in Figure 9c. The Mg peaks were converted to MgH_2, revealing that the hydrogen absorption process had completely occurred. However, the peak of CoO, La_2O_3, and MgO were still detected. The following equation (Equation (3)) can be used to predict the reaction between 10 wt.% of $LaCoO_3$ with MgH_2:

$$MgH_2 + 2LaCoO_3 \rightarrow 2CoO + La_2O_3 + MgO + H_2 \quad (3)$$

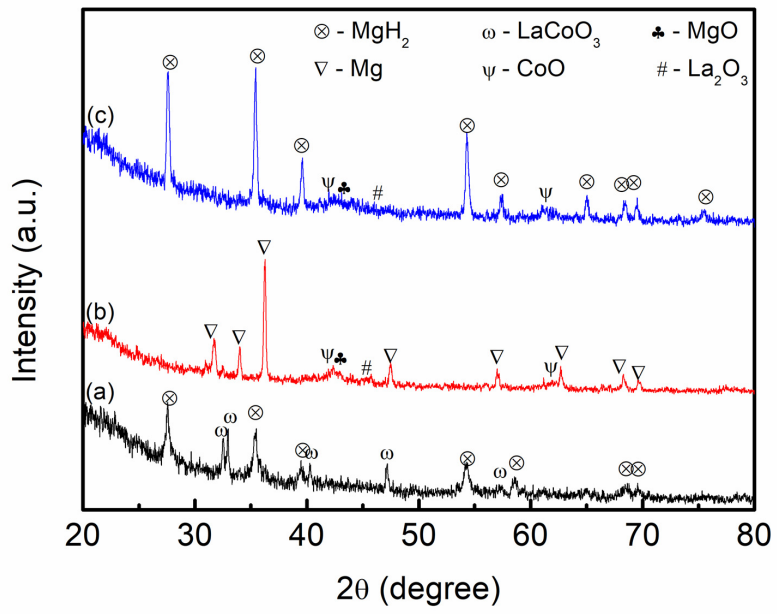

Figure 9. XRD pattern of 10 wt.% of $LaCoO_3$ with MgH_2 (a) milled for 1 h, (b) after desorption temperature at 450 °C, and (c) after absorption at 250 °C.

A prior study conducted by Rahman et al. [42] discovered that adding $KNbO_3$ greatly reduced the onset desorption temperature from 370 °C to 327 °C, and lowered the E_A by 61 kJ/mol, when compared with milled MgH_2. Additionally, when as-synthesized Co@C was added to MgH_2, the desorption temperature was reduced by 99 °C compared with milled MgH_2 [43]. Furthermore, at 300 °C, MgH_2-Co@C composites absorbed 5.96 wt.% of H_2 in 10 min, and desorbed 5.74 wt.% of H_2 in 1 h. Another metal oxide catalyst, $SrFe_{12}O_{19}$, also exhibited superior performance for MgH_2 [6]. In comparison to milled MgH_2, the introduction of $SrFe_{12}O_{19}$ decreased the E_A and onset desorption temperature from 350 °C to 270 °C, and 133.31 kJ/mol to 114.22 kJ/mol, respectively. According to the findings, the in-situ formation of SrO, $MgFe_2O_4$, and Fe plays a crucial role in enhancing the hydrogen storage properties of MgH_2. In this study, according to the results of the onset desorption temperature, ab/desorption kinetics, and the activation energy, adding the $LaCoO_3$ (metal oxides) additive greatly enhances the hydrogen storage performance of MgH_2. The onset desorption temperature was reduced by 28 °C and the E_A was lowered by 43 kJ/mol. In addition, this composite could absorb 7.30 wt.% of H_2 at 250 °C and desorb 3.24 wt.% of H_2 at 300 °C, which is faster in kinetics compared with milled MgH_2. The further study exposed that in situ-generated CoO, La_2O_3, and MgO could play a significant role in enhancing the dehydrogenation performance of MgH_2.

According to Lee et al. [52], adding CoO has the best impact on the hydrogen sorption properties of Mg. Reactive grinding of Mg with Co/CoO causes defects and cracks in the surface of Mg particles, thus shortening diffusion distances between the samples. In addition, adding a minimal amount of CoO diminishes the dehydrogenation temperature and speeds up the dehydrogenation rate of $LiBH_4.NH_3$–3LiH system [53]. Furthermore, adding La_2O_3 to MgH_2 improves the sorption properties [54]. Our previous study [19] also found that the introduction of 10 wt.% $LaFeO_3$ positively affected the sorption kinetics of MgH_2. After the addition of $LaFeO_3$, the E_A decreased by 32 kJ/mol. Besides this, when MgH_2 was milled with MgO, the hydrogen kinetics were dramatically improved compared with MgH_2 [55]. At 300 °C, faster hydrogen absorption and desorption kinetics can be accomplished in <100 s. Based on the discussions above, the introduction of $LaCoO_3$ lowered the onset desorption temperature and enhanced the kinetic properties of MgH_2 via the formation of in situ-generated CoO, La_2O_3, and MgO.

4. Conclusions

In conclusion, the different weight percentages of $LaCoO_3$ have different effects on the hydrogen storage performance of MgH_2. In comparison to milled and pure MgH_2, the addition of $LaCoO_3$ allows hydrogen to be released at a lower temperature. For 5 wt.%, 10 wt.%, 15 wt.%, and 20 wt.% of $LaCoO_3$-doped MgH_2 composites, the composites decomposed at 316 °C, 322 °C, 310 °C, and 323 °C, respectively, which were at lower temperatures than those of milled MgH_2 and pure MgH_2. In the reversibility evaluation, 5 wt.%, 10 wt.%, 15 wt.%, and 20 wt.% of $LaCoO_3$-doped MgH_2 samples absorbed 7.30 wt.%, 7.30 wt.%, 6.99 wt.%, and 5.49 wt.%, respectively, at 250 °C within 20 min. Meanwhile, milled MgH_2 could absorb less than 6.68 wt.% of H_2 under the same conditions. In addition, the isothermal desorption kinetics for 5 wt.%, 10 wt.%, 15 wt.%, and 20 wt.% of $LaCoO_3$-doped MgH_2 were 2.46 wt.%, 3.24 wt.%, 2.04 wt.%, and 4.53 wt.%, respectively, which were higher than that of milled MgH_2 (0.34 wt.%). Through the DSC and Kissinger equation, the activation energy of 10 wt.% of $LaCoO_3$ with MgH_2 was 90 kJ/mol, which was 43 kJ/mol lower than that of milled MgH_2. Furthermore, the doped samples present a smaller particle size compared with pure and milled MgH_2, which allows more hydrogen to be absorbed/released. According to the XRD results, the in-situ formation of CoO, La_2O_3, and MgO plays a synergistic role in significantly improving MgH_2 hydrogen storage performance.

Author Contributions: N.S., Writing—original draft, methodology; M.F.M.D., writing—review and editing; M.I., supervision, writing—original draft; S.-U.R., writing—review and editing; H.S.B., writing—review and editing; H.A., writing—review and editing; A.A.T., writing—review and editing; U.S., writing—review and editing. All authors have read and agreed to the published version of the manuscript.

Funding: This research was funded by Institutional Fund Projects under grant no. (IFPIP: 408-135-1443).

Institutional Review Board Statement: Not applicable.

Informed Consent Statement: Not applicable.

Data Availability Statement: The data presented in this study are available on request from the corresponding author.

Acknowledgments: The authors gratefully acknowledge technical and financial support provided by the Ministry of Education and King Abdulaziz University, DSR, Jeddah, Saudi Arabia.

Conflicts of Interest: The authors declare no conflict of interest.

References

1. Gong, L.; Xuan, N.; Gu, G.; Lv, P.; Huang, N.; Song, C.; Zheng, M.; Wang, J.; Cui, P.; Gu, G.; et al. Power management and system optimization for high efficiency self-powered electrolytic hydrogen and formic acid production. *Nano Energy* **2023**, *107*, 108124. [CrossRef]
2. Le, S.T.; Nguyen, T.N.; Linforth, S.; Ngo, T.D. Safety investigation of hydrogen energy storage systems using quantitative risk assessment. *Int. J. Hydrogen Energy* **2023**, *48*, 2861–2875. [CrossRef]
3. Xu, Y.; Deng, Y.; Liu, W.; Zhao, X.; Xu, J.; Yuan, Z. Research progress of hydrogen energy and metal hydrogen storage materials. *Sustain. Energy Technol. Assess* **2023**, *55*, 102974. [CrossRef]
4. Zhang, L.; Nyahuma, F.M.; Zhang, H.; Cheng, C.; Zheng, J.; Wu, F.; Chen, L. Metal organic framework supported niobium pentoxide nanoparticles with exceptional catalytic effect on hydrogen storage behavior of MgH_2. *Green Energy Environ.* **2023**, *8*, 589–600. [CrossRef]
5. Wan, C.; Zhou, L.; Xu, S.; Jin, B.; Ge, X.; Qian, X.; Xu, L.; Chen, F.; Zhan, X.; Yang, Y.; et al. Defect engineered mesoporous graphitic carbon nitride modified with AgPd nanoparticles for enhanced photocatalytic hydrogen evolution from formic acid. *Chem. Eng. J.* **2022**, *429*, 132388. [CrossRef]
6. Mustafa, N.S.; Sulaiman, N.N.; Ismail, M. Effect of $SrFe_{12}O_{19}$ nanopowder on the hydrogen sorption properties of MgH_2. *RSC Adv.* **2016**, *6*, 110004–110010. [CrossRef]
7. Zhang, M.; Xiao, X.; Luo, B.; Liu, M.; Chen, M.; Chen, L. Superior de/hydrogenation performances of MgH_2 catalyzed by 3D flower-like TiO_2@C nanostructures. *J. Energy Chem.* **2020**, *46*, 191–198. [CrossRef]
8. Yartys, V.; Lototskyy, M.; Akiba, E.; Albert, R.; Antonov, V.; Ares, J.; Baricco, M.; Bourgeois, N.; Buckley, C.; von Colbe, J.B.; et al. Magnesium based materials for hydrogen based energy storage: Past, present and future. *Int. J. Hydrogen Energy* **2019**, *44*, 7809–7859. [CrossRef]
9. Iyakutti, K.; Surya, V.J.; Lavanya, R.; Vasu, V.; Rajeswarapalanichamy, R.; Kawazoe, Y. Effects of nanostructures on the hydrogen storage properties of MgH_2—A first principles study. *Comput. Condens. Matter* **2022**, *30*, e00643. [CrossRef]
10. Liang, G.; Huot, J.; Boily, S.; Van Neste, A.; Schulz, R. Hydrogen storage properties of the mechanically milled MgH_2–V nanocomposite. *J. Alloys Compd.* **1999**, *291*, 295–299. [CrossRef]
11. Ren, L.; Zhu, W.; Zhang, Q.; Lu, C.; Sun, F.; Lin, X.; Zou, J. MgH_2 confinement in MOF-derived N-doped porous carbon nanofibers for enhanced hydrogen storage. *Chem. Eng. J.* **2022**, *434*, 134701. [CrossRef]
12. Sazelee, N.; Ali, N.A.; Yahya, M.S.; Mustafa, N.S.; Halim Yap, F.A.; Mohamed, S.B.; Ghazali, M.Z.; Suwarno, S.; Ismail, M. Recent advances on Mg–Li–Al systems for solid-state hydrogen storage: A Review. *Front. Energy Res.* **2022**, *10*, 875405. [CrossRef]
13. Friedrichs, O.; Aguey-Zinsou, F.; Fernández, J.A.; Sánchez-López, J.; Justo, A.; Klassen, T.; Bormann, R.; Fernández, A. MgH_2 with Nb_2O_5 as additive, for hydrogen storage: Chemical, structural and kinetic behavior with heating. *Acta Mater.* **2006**, *54*, 105–110. [CrossRef]
14. Shao, Y.; Gao, H.; Tang, Q.; Liu, Y.; Liu, J.; Zhu, Y.; Zhang, J.; Li, L.; Hu, X.; Ba, Z. Ultra-fine TiO_2 nanoparticles supported on three-dimensionally ordered macroporous structure for improving the hydrogen storage performance of MgH_2. *Appl. Surf. Sci.* **2022**, *585*, 152561. [CrossRef]
15. Huang, X.; Xiao, X.; Wang, X.; Wang, C.; Fan, X.; Tang, Z.; Wang, C.; Wang, Q.; Chen, L. Synergistic catalytic activity of porous rod-like $TMTiO_3$ (TM= Ni and Co) for reversible hydrogen storage of magnesium hydride. *J. Phys. Chem. C* **2018**, *122*, 27973–27982. [CrossRef]
16. Zhang, J.; Hou, Q.; Guo, X.; Yang, X. Achieve high-efficiency hydrogen storage of MgH_2 catalyzed by nanosheets $CoMoO_4$ and rGO. *J. Alloys Compd.* **2022**, *911*, 165153. [CrossRef]
17. Zhang, J.; Hou, Q.; Chang, J.; Zhang, D.; Peng, Y.; Yang, X. Improvement of hydrogen storage performance of MgH_2 by $MnMoO_4$ rod composite catalyst. *Solid. State Sci.* **2021**, *121*, 106750. [CrossRef]

18. Ismail, M. Effect of $LaCl_3$ addition on the hydrogen storage properties of MgH_2. *Energy* **2015**, *79*, 177–182. [CrossRef]
19. Sazelee, N.A.; Idris, N.H.; Md Din, M.F.; Yahya, M.S.; Ali, N.A.; Ismail, M. $LaFeO_3$ synthesised by solid-state method for enhanced sorption properties of MgH_2. *Results Phys.* **2020**, *16*, 102844. [CrossRef]
20. Soni, P.K.; Bhatnagar, A.; Shaz, M.A.; Srivastava, O.N. Effect of graphene templated fluorides of Ce and La on the de/rehydrogenation behavior of MgH_2. *Int. J. Hydrogen Energy* **2017**, *42*, 20026–20035. [CrossRef]
21. Wu, C.; Wang, Y.; Liu, Y.; Ding, W.; Sun, C. Enhancement of hydrogen storage properties by in situ formed LaH_3 and Mg_2NiH_4 during milling MgH_2 with porous $LaNiO_3$. *Catal. Today* **2018**, *318*, 113–118. [CrossRef]
22. Zhang, L.; Lu, X.; Sun, Z.; Yan, N.; Yu, H.; Lu, Z.; Zhu, X. Superior catalytic effect of facile synthesized $LaNi_{4.5}Mn_{0.5}$ submicro-particles on the hydrogen storage properties of MgH_2. *J. Alloys Compd.* **2020**, *844*, 156069. [CrossRef]
23. Juahir, N.; Mustafa, N.; Sinin, A.; Ismail, M. Improved hydrogen storage properties of MgH_2 by addition of Co_2NiO nanoparticles. *RSC Adv.* **2015**, *5*, 60983–60989. [CrossRef]
24. Zhang, J.; Shan, J.; Li, P.; Zhai, F.; Wan, Q.; Liu, Z.; Qu, X. Dehydrogenation mechanism of ball-milled MgH_2 doped with ferrites ($CoFe_2O_4$, $ZnFe_2O_4$, $MnFe_2O_4$ and $Mn_{0.5}Zn_{0.5}Fe_2O_4$) nanoparticles. *J. Alloys Compd.* **2015**, *643*, 174–180. [CrossRef]
25. Cabo, M.; Garroni, S.; Pellicer, E.; Milanese, C.; Girella, A.; Marini, A.; Rossinyol, E.; Suriñach, S.; Baró, M.D. Hydrogen sorption performance of MgH_2 doped with mesoporous nickel- and cobalt-based oxides. *Int. J. Hydrogen Energy* **2011**, *36*, 5400–5410. [CrossRef]
26. Mandzhukova, T.; Khrussanova, M.; Grigorova, E.; Stefanov, P.; Khristov, M.; Peshev, P. Effect of $NiCo_2O_4$ additives on the hydriding properties of magnesium. *J. Alloys Compd.* **2008**, *457*, 472–476. [CrossRef]
27. Liu, B.; Zhang, B.; Chen, X.; Lv, Y.; Huang, H.; Yuan, J.; Lv, W.; Wu, Y. Remarkable enhancement and electronic mechanism for hydrogen storage kinetics of Mg nano-composite by a multi-valence Co-based catalyst. *Mater. Today Nano* **2022**, *17*, 100168. [CrossRef]
28. Sarker, A.R. Synthesis of high quality $LaCoO_3$ crystals using water based sol-gel method. *Int. J. Mater. Sci. Appl.* **2015**, *4*, 159–164.
29. Ajmal, S.; Bibi, I.; Majid, F.; Ata, S.; Kamran, K.; Jilani, K.; Nouren, S.; Kamal, S.; Ali, A.; Iqbal, M. Effect of Fe and Bi doping on $LaCoO_3$ structural, magnetic, electric and catalytic properties. *J. Mater. Res. Technol.* **2019**, *8*, 4831–4842. [CrossRef]
30. Worayingyong, A.; Kangvansura, P.; Ausadasuk, S.; Praserthdam, P. The effect of preparation: Pechini and Schiff base methods, on adsorbed oxygen of $LaCoO_3$ perovskite oxidation catalysts. *Colloids Surf. A Physicochem. Eng. Asp.* **2008**, *315*, 217–225. [CrossRef]
31. Radev, L.; Pavlova, L.; Samuneva, B.; Kashchieva, E.; Mihailova, I.; Zaharescu, M.; Malic, B.; Predoana, L. Sol-gel synthesis and structure of La_2O_3-CoO-SiO_2 powders. *Process Appl. Ceram.* **2008**, *2*, 103–108. [CrossRef]
32. Wang, N.; Liu, J.; Gu, W.; Song, Y.; Wang, F. Toward synergy of carbon and La_2O_3 in their hybrid as an efficient catalyst for the oxygen reduction reaction. *RSC Adv.* **2016**, *6*, 77786–77795. [CrossRef]
33. Prado-Gonjal, J.; Schmidt, R.; Morán, E. Microwave assisted synthesis and characterization of perovskite oxides. *ChemInform* **2014**, *45*, 117–140. [CrossRef]
34. Shokano, G.; Dehouche, Z.; Galey, B.; Postole, G. Development of a novel method for the fabrication of nanostructured $Zr_{(x)}Ni_{(y)}$ catalyst to enhance the desorption properties of MgH_2. *Catalysts* **2020**, *10*, 849. [CrossRef]
35. Pandey, S.K.; Bhatnagar, A.; Shahi, R.R.; Hudson, M.; Singh, M.K.; Srivastava, O. Effect of TiO_2 nanoparticles on the hydrogen sorption characteristics of magnesium hydride. *J. Nanosci. Nanotechnol.* **2013**, *13*, 5493–5499. [CrossRef]
36. Ranjbar, A.; Guo, Z.P.; Yu, X.B.; Wexler, D.; Calka, A.; Kim, C.J.; Liu, H.K. Hydrogen storage properties of MgH_2–SiC composites. *Mater. Chem. Phys.* **2009**, *114*, 168–172. [CrossRef]
37. Sulaiman, N.; Mustafa, N.; Ismail, M. Effect of Na_3FeF_6 catalyst on the hydrogen storage properties of MgH_2. *Dalton Trans.* **2016**, *45*, 7085–7093. [CrossRef] [PubMed]
38. Lozano, G.A.; Ranong, C.N.; Bellosta von Colbe, J.M.; Bormann, R.; Fieg, G.; Hapke, J.; Dornheim, M. Empirical kinetic model of sodium alanate reacting system (I). Hydrogen absorption. *Int. J. Hydrogen Energy* **2010**, *35*, 6763–6772. [CrossRef]
39. Ismail, M.; Mustafa, N.S.; Juahir, N.; Halim Yap, F.A. Catalytic effect of $CeCl_3$ on the hydrogen storage properties of MgH_2. *Mater. Chem. Phys.* **2016**, *170*, 77–82. [CrossRef]
40. Yahya, M.S.; Sulaiman, N.N.; Mustafa, N.S.; Halim Yap, F.A.; Ismail, M. Improvement of hydrogen storage properties in MgH_2 catalysed by K_2NbF_7. *Int. J. Hydrogen Energy* **2018**, *43*, 14532–14540. [CrossRef]
41. Verma, S.K.; Shaz, M.A.; Yadav, T.P. Enhanced hydrogen absorption and desorption properties of MgH_2 with graphene and vanadium disulfide. *Int J Hydrogen Energy* 2022, *in press*. [CrossRef]
42. Rahman, M.H.A.; Shamsudin, M.A.; Klimkowicz, A.; Uematsu, S.; Takasaki, A. Effects of $KNbO_3$ catalyst on hydrogen sorption kinetics of MgH_2. *Int. J. Hydrogen Energy* **2019**, *44*, 29196–29202. [CrossRef]
43. Li, L.; Jiang, G.; Tian, H.; Wang, Y. Effect of the hierarchical Co@C nanoflowers on the hydrogen storage properties of MgH_2. *Int. J. Hydrogen Energy* **2017**, *42*, 28464–28472. [CrossRef]
44. Czujko, T.; Oleszek, E.E.; Szot, M. New aspects of MgH_2 morphological and structural changes during high-energy ball milling. *Mater* **2020**, *13*, 4550. [CrossRef]
45. Shang, Y.; Pistidda, C.; Gizer, G.; Klassen, T.; Dornheim, M. Mg-based materials for hydrogen storage. *J. Magnes Alloy* **2021**, *9*, 1837–1860. [CrossRef]
46. Chawla, K.; Kumar Yadav, D.; Bajpai, A.; Kumar, S.; Jain, I.P.; Lal, C. Effect of $PdCl_2$ catalyst on the hydrogenation properties and sorption kinetics of Mg. *Sustain. Energy Technol. Assess* **2022**, *51*, 101981. [CrossRef]

47. Aguey-Zinsou, K.F.; Nicolaisen, T.; Ares Fernandez, J.R.; Klassen, T.; Bormann, R. Effect of nanosized oxides on MgH_2 (de)hydriding kinetics. *J. Alloys Compd.* **2007**, *434–435*, 738–742. [CrossRef]
48. Xiao, X.; Liu, Z.; Saremi-Yarahmadi, S.; Gregory, D.H. Facile preparation of β-/γ-MgH_2 nanocomposites under mild conditions and pathways to rapid dehydrogenation. *Phys. Chem. Chem. Phys.* **2016**, *18*, 10492–10498. [CrossRef] [PubMed]
49. Rahmaninasab, M.A.; Raygan, S.; Abdizadeh, H.; Pourabdoli, M.; Mirghaderi, S.H. Properties of activated $MgH_2$$^+$ mischmetal nanostructured composite produced by ball-milling. *Mater. Renew. Sustain. Energy* **2018**, *7*, 15. [CrossRef]
50. Si, T.Z.; Zhang, X.Y.; Feng, J.J.; Ding, X.L.; Li, Y.T. Enhancing hydrogen sorption in MgH_2 by controlling particle size and contact of Ni catalysts. *Rare Met.* **2021**, *40*, 995–1002. [CrossRef]
51. Zhang, Q.; Huang, Y.; Xu, L.; Zang, L.; Guo, H.; Jiao, L.; Yuan, H.; Wang, Y. Highly dispersed MgH_2 nanoparticle-graphene nanosheet composites for hydrogen storage. *ACS Appl. Nano Mater.* **2019**, *2*, 3828–3835. [CrossRef]
52. Lee, D.; Kwon, I.; Bobet, J.L.; Song, M.Y. Effects on the H_2-sorption properties of Mg of Co (with various sizes) and CoO addition by reactive grinding. *J. Alloys Compd.* **2004**, *366*, 279–288. [CrossRef]
53. Zhang, Y.; Liu, Y.; Zhang, X.; Li, Y.; Gao, M.; Pan, H. Mechanistic understanding of CoO-catalyzed hydrogen desorption from a $LiBH_4$·NH_3–3LiH system. *Dalton Trans.* **2015**, *44*, 14514–14522. [CrossRef] [PubMed]
54. Gupta, R.; Agresti, F.; Russo, S.L.; Maddalena, A.; Palade, P.; Principi, G. Structure and hydrogen storage properties of MgH_2 catalysed with La_2O_3. *J. Alloys Compd.* **2008**, *450*, 310–313. [CrossRef]
55. Ares Fernández, J.R.; Aguey Zinsou, K.F. Superior MgH_2 kinetics with MgO addition: A tribological effect. *Catalysts* **2012**, *2*, 330–343. [CrossRef]